7-1-2022

The interaction and orientation of Peptide KL4 in model membranes

Drew Marquardt
University of Windsor

Brad van Oosten
Brock University

Maksymilian Dziura
University of Windsor

Joanna R. Long
University of Florida

Thad A. Harroun
Brock University

The interaction and orientation of Peptide KL_4 in model membranes

Drew Marquardt,[*,†,‡] Brad van Oosten,[¶] Maksymilian Dziura,[†] Joanna R. Long,[§] and Thad A. Harroun[*,¶]

†*Department of Chemistry and Biochemistry, University of Windsor, Windsor, Ontario, Canada*

‡*Department of Physics, University of Windsor, Windsor, Ontario, Canada*

¶*Department of Physics, Brock University, St. Catharines, Ontario, Canada*

§*Department of Biochemistry and Molecular Biology, University of Florida, Gainesville, Florida, USA.*

E-mail: drew.marquardt@uwindsor.ca; thad.harroun@brocku.ca

Abstract

We report on the orientation and location of synthetic pulmonary surfactant peptide KL_4, $(KLLLL)_4K$, in model lipid membranes. The partitioning depths of selectively deuterated leucine residues within KL_4 were determined in DPPC:POPG (4:1) and POPC:POPG (4:1) bilayers by oriented neutron diffraction. These measurements were combined with an NMR-generated model of the peptide structure to determine the orientation and partitioning of the peptide at the lipid-water interface. The results demonstrate KL_4 adopting an orientation that interacts with a single membrane leaflet. These observations are consistent with past ^2H NMR and EPR studies [Antharam *et al., Biophysical Journal*, 2009, **96**, 4085; Turner *et al., BBA-Biomembranes*, 2014].

1. Introduction

One of the remarkable phenomena in the process of respiration is the role of the fluid coating the walls of the lung's alveoli called pulmonary surfactant (PS).[1] The role of the pulmonary surfactant is to lower the surface tension of the alveoli making possible the inflation of the alveoli with only about 1 Torr of pressure over the surroundings.[1] The success of a newborn's first breath depends upon this surfactant and thus incomplete formation of any component of the pulmonary surfactant makes this breath more difficult, specifically in premature infants.[2] This condition is known as infant respiratory distress syndrome (IRDS).[3]

Pulmonary surfactant is a mixture of both lipids and proteins, where compositions may vary according to species. The main constituent pulmonary surfactants is the phospholipid dipalmitoyl phosphatidylcholine (DPPC) however there are other lipid components including: unsaturated phosphatidylcholines (PC) and phosphatidylglycerols (PG).[4] Natural pulmonary surfactant also contain surfactant specific proteins, known as surfactant proteins (SP) and include: SP-A, SP-B, SP-C and SP-D.[1,5,6] In an effort to combat IRDS synthetic surfactant protein mimics have been developed. One example is the peptide KL_4, which was synthesized with a ratio of cationic to hydrophobic residues similar to that of SP-B, a vital protein in the pulmonary surfactant system.[7] The structures of KL_4 and the aforementioned lipids are all visualized in Figure 1.

Lung surfactant protein B (SP-B) is an essential protein for lowering surface tension in the alveoli.[8] The native form of SP-B is highly hydrophobic and contains 7 disulfide bridges which make pharmaceutical expression of the protein in large quantities problematic. Animal derived PS formulations have been very successfully used to combat respiratory distress syndrome (RDS) in premature infants, but they raise concerns regarding purity, immunogenicity, and uniformity.[9] Thus, synthetic replacements of SP-B have been highly sought after. KL_4 (sinapultide, Sequence: $(KLLLL)_4K$) is a 21-residue peptide mimic of SP-B which has proven to clinically successful in relieving RDS when administered in a phospholipid dispersion.[10] Lucinactant is one medically-produced pulmonary surfactant, which incorporates sinapul-

tide in its formula.[10] The focus of this research is on the biophysical properties of KL_4 and their relation to alleviating RDS. Notably, KL_4 retains many of the macroscopic properties of SP-B despite bearing little sequence similarity. Understanding how the comparatively simple KL_4 is so successful will lead to a better understanding of SP-B and better synthetic analogues.[11]

Initially, the compositions of DPPC:POPG (palmitoyl-oleoyl PG) (4:1) and POPC (palmitoyl-oleoyl PC):POPG (4:1) will be examined. These lipid compositions are chosen to mimic the formulations used in past lung surfactant studies; in addition the second is a common composition for the study of membrane active peptides.[11,12]

An ongoing difficulty in the study of membrane bound proteins and peptides is their inability to be studied outside of the membrane and propensity to adopt different secondary structures depending on the lipid species composing the membrane. As a result of this difficulty the orientation of KL_4 in model membranes has been a point of uncertainty in literature, specifically whether the peptide adopts a transmembrane orientation.[13]

Currently a debate exists on whether KL_4 is a transmembrane helix or whether it aligns itself with the plane of the bilayer at the lipid —water interface. This inconsistency in literature could be a consequence of choice of model membrane composition, or technique available to interrogate the system. In an effort to determine the orientation of KL_4's interaction with membranes, past studies have been conducted which include: NMR, circular dichroism, and differential scanning calorimetry (DSC). The results of such experiments have yielded inconclusive results, primarily due to the employed techniques focusing on the bulk properties of the system.[11,14,15] In this study neutron diffraction was employed to determine the orientation of KL_4 based on three selectively deuterium labeled KL_4 samples. Deuterium–hydrogen substitution provides a probe free method of contrast commonly used to determine the location of small membrane bound molecules.[16–18]

In this article, we use experimentally determined label locations of specific Leucine residues as well as calculations to determine the most probable position and orientation

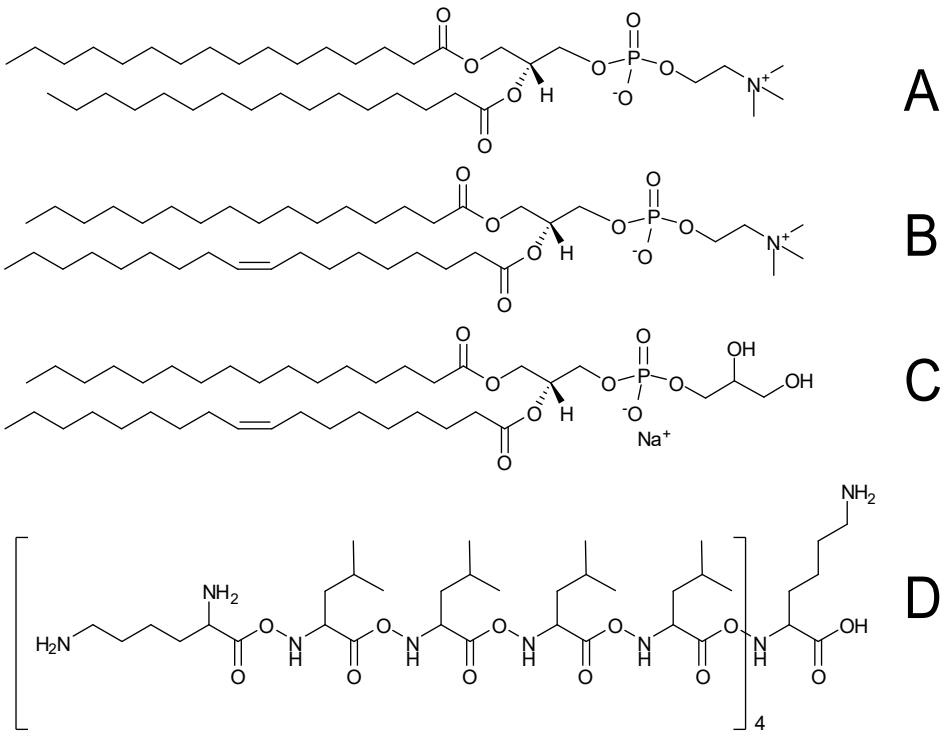

Figure 1: Structures of (**A**) di-palmitoyl phosphatidylcholine (16:0-16:0 PC, DPPC), (**B**) palmitoyl-oleoyl phosphatidylcholine (16:0-18:1 PC, POPC) ,(**C**) palmitoyl-oleoyl phosphatidylglycerol (16:0-18:1 PG, POPG), and (**D**) peptide KL_4.

of KL_4 in two model membrane systems.

2. Material and Methods

Di-palmitoyl (16:0-16:0PC) and palmitoyl-oleoyl (16:0-18:1PC) phosphocholine, and palmitoyl-oleoyl phosphoglycerol were purchased from Avanti Polar Lipids (Alabaster, AL). The lipids were mixed in chloroform and aliquoted. Selectively deuterated 5-d_3-L-leucine was purchased (Cambridge Isotopes, Andover, MA) and fmoc-protected using standard protocols. Three variants of KL_4, each containing a single enriched leucine (L3, L12, or L19), were synthesized via solid-phase peptide synthesis on a Wang resin (ABI 430, ICBR, UF), cleaved from the resin with TFA/triisopropyl-silane/water and ether precipitated. The cleaved product was purified via RP-HPLC using a C18 Vydac column with a water/acetonitrile gradient. The fractions corresponding to KL_4 were collected and purity of the product was verified by mass spectrometry with a single species of MW=2572. Dried peptide dissolved in methanol to a stock concentration of approximately 1 mM, and aliquots were analyzed by amino acid analysis for a more accurate determination of concentration (Molecular Structure Facility, UC Davis).

2.1 Neutron Scattering

The methods of sample preparation and neutron diffraction follow those described previously.[19,20] All preparations of aligned multilayer samples were carried out in a nitrogen environment. A total of 12 mg of phospholipid was mixed with 5 mol % KL_4 by mixing the chloroform and methanol stock solutions. The mixture was deposited on a silicon single crystal substrate, and the solvent evaporated while gently rocking the sample. This produces well aligned lamellar samples in a reproducible manner. The samples were then placed in a vacuum for $\sim$6 h to remove traces of the solvent. The samples were then sealed into sample holders and equilibrated in a humid nitrogen atmosphere at room temperature for several

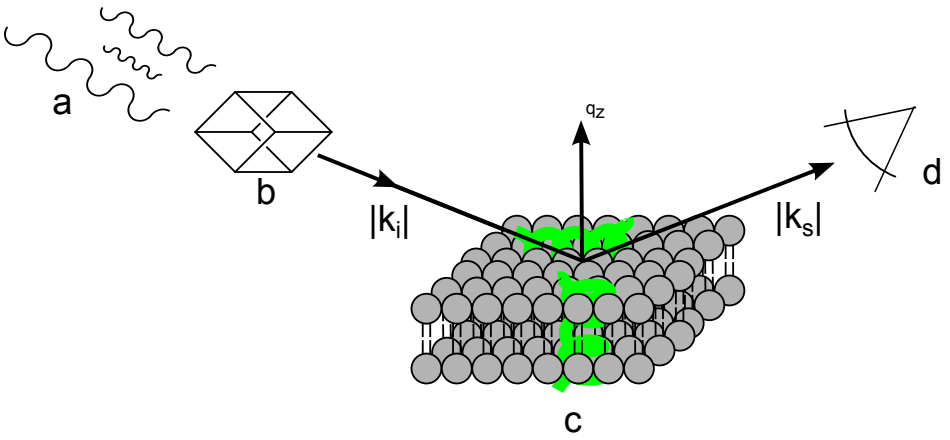

Figure 2: Schematic diagram of neutron diffraction. **a**) A "white" beam of neutrons, **b**) monochromator selects a single wavelength of neutrons. $|k_i|$ is the incident vector of monochromatic neutron beam and $|k_s|$ is the vector of scattered neutrons of the same energy ($|k_i|=|k_s|$). **c**) is the model membrane sample oriented such that the scattering vector (q_z) is perpendicular to the bilayer surface and **d**) is a multiwire 1-dimensional detector.

hours. Samples were hydrated at fixed humidity using a saturated salt solution of KNO_3 (94 % relative humidity) with 0, 8, 16 or 40, or 70 mol% ^2H_2O. Samples were kept at room temperature during initial equilibration and at 37±0.5 ^oC during data collection.

Neutron diffraction data were collected on the N5 and D3 beam-lines at the Canadian Neutron Beam Center (CNBC, Chalk River, Ontario, Canada) at a wavelength of 2.37 Åusing a single crystal monochromator. Typically four to five pseudo-Bragg peaks were recorded, and the reconstructed unit cell has a canonical resolution of 9-11 Å. Data corrections and reconstruction of the bilayer profile proceeded as outlined in a previous paper.[20] The SLD profile ρ(z) was constructed with the cosine transform of the measured form factors F_h, Eqn 1. The difference between labeled and unlabeled neutron data were calculated with of the difference in the measured form factors; $F_h = F_h^L - F_h^U$. Data were placed on an absolute scale by first calculating the total SLD of the unit cell, in units of $Å^{-2}mol^{-1}$, for every sample condition.

$$\rho(z) = \frac{2}{d}\sum_{h=1}^{h_{max}} F_h cos(\frac{2h\pi z}{d}) \tag{1}$$

2.2 Data Analysis

The data analysis is carried out in a similar fashion to previous studies determining the location of cholesterol.[20,21] The diffraction peaks were obtained from $\theta - 2\theta$ scans where the Bragg condition was satisfied (Eqn. 2); θ and 2θ are the angles of the sample and the detector, respectively.

$$n\lambda = 2dsin(\theta) \tag{2}$$

The integrated intensities of the quasi-Bragg peaks are the uncorrected square of discreet form factors from the bilayer. To these intensities three corrections are applied : the flux correction (C_{flux}), the absorbance correction (C_{abs}) and the Lorentz correction (C_{Lor}). C_{flux} (eqn. 3) corrects for the geometry of the sample rotation with respect to the beam.

$$C_{flux} = \frac{1}{sin(\theta)} \tag{3}$$

C_{abs} (eqn. 4) corrects for the neutrons absorbed by the sample, where μ is the total absorbance cross section of the sample and t is the sample thickness. μ is calculated by considering all of the atoms present in a unit cell which is typically a one lipid wide slice of the bilayer with the appropriate water per lipid and percentage of the guest molecule.

$$C_{abs} = \frac{\alpha}{1 - e^{-\alpha}} \tag{4}$$

$$\alpha = \frac{2\mu t}{sin(\theta)} \tag{5}$$

C_{Lor} (eqn. 6) is the correction for angular velocity:

$$C_{Lor} = sin(2\theta) \tag{6}$$

The final form factor is determined by taking the square of the corrected diffraction

intensities.

$$F_h = \sqrt{C_{flux} C_{abs} C_{Lor} I_h} \tag{7}$$

The corrected form factors are then applied in a cosine Fourier sum to produce a map of neutron scattering length density (ρ) in real space, analogous to an electron density map determined by X-ray crystallography,

$$\rho = \frac{F_o}{d} + \frac{2}{d} \sum_{h=1}^{h} F_h cos(\frac{2\pi h z}{d}) \tag{8}$$

where d represents the repeat spacing of the unit cell, h is the diffraction order and F_o is the total scattering length of the unit cells (the unit cell cannot be measured so it is calculated based on scattering length of all atoms in the system).

$$\Delta\rho = \frac{F_o^L - F_o^U}{d} + \frac{2}{d} \sum_{h=1}^{h} (F_h^L - F_h^U) cos(\frac{2\pi h z}{d}) \tag{9}$$

The difference in scattering length density between samples ($\Delta\rho$, eqn. 10) is determined by a cosine reconstruction using the difference between labeled and unlabeled corrected form factors, measured using deuterated and undeuterated peptides, F_h^L and F_h^U respectively. A Gaussian model (1 or 2 Gaussians) was fit to $\Delta\rho$. Fitting a model to $\Delta\rho$ serves two purposes: i) it allows for quantification of label distributions and ii) it allows the labeled and unlabeled data to be scaled relative to each other as our neutron data was scaled in reciprocal space using the Hristova scaling method. The Gaussian model follows eqn. 10:

$$F_h^L = A e^{-(\pi\sigma h/d)^2} cos(\frac{2\pi h z_o}{d}), \tag{10}$$

where σ is the distribution width, z_o is the centre of the distribution and A=$F_o^L - F_o^U$. To scale the data sets, eqn. 9 (modified with two scaling factors k^L and k^U) is equated to the cosine transform of eqn. 10

$$\frac{2}{d}\sum_{h=1}^{h}(F_h^L)cos(\frac{2\pi hz}{d}) = \frac{2}{d}\sum_{h=1}^{h}(\frac{F_h^L}{k^L} - \frac{F_h^U}{k^U})cos(\frac{2\pi hz}{d})$$

$$\sum_{h=1}^{h}((\frac{F_h^L}{k^L} - \frac{F_h^U}{k^U}) - F_h^L)cos(\frac{2\pi hz}{d}) = 0 \tag{11}$$

The result (eqn. 11) is a set of equations (h = 1, 2, 3...) and four unknowns (k^L, k^U, σ, z_o). The parameter A is the only assumed parameter, and is based on the known sample composition.

To test of the quality of our model, we introduce the commonly used concept of a crystallography R-factor.[22] However, our model is constructed from eqn. 10 which relies on the *difference* between labeled and unlabeled form factors, so we modify the standard R-factor from :

$$R = \frac{\sum F_h^{obs} - F_h^{calc}}{\sum F_h^{obs}} \tag{12}$$

to the modified R-fatcter, R_{mod}:

$$R_{mod} = \frac{\sum(F_h^L - F_h^U) - \Delta F_h^{calc}}{\sum(F_h^L - F_h^U)}. \tag{13}$$

We do not expect R_{mod} values as small as R-factors observed with x-ray crystallography of solid crystals as the multilamellar phospholipid stacks are highly fluid and contain many imperfections.

2.3 Orientation Optimization

By adopting experimental parameters, this method calculates the energy cost due to the effects of hydrophobic interactions of the protein with the lipid-water interface. This method tests a continuum of orientations of the peptide which fit our experimental parameters to

determine the lowest energy orientation.

The water profile from the neutron scattering experiments was used to create a penalty function based on the hydrophobicity of each atom in the protein. The experimentally determined parameters of the centre of the water layer, at $\pm z_o$ Å relative to the bilayer centre, as well as the variance, σ, were taken from the scattering experiments to create the penalty function, Eqn 14. This function ranges from -0.5 in the most hydrophobic region to 0.5 in the most hydrophilic region of the bilayer.

$$C(z) = -0.5 + e^{1/2\frac{ZZ_o}{\sigma^2}} \tag{14}$$

To quantify the effects of the atoms interacting with the lipid-water interface, the solvent accessible surface area and the transfer energy of each atom were calculated using results taken from Ducarme *et al.* regarding the transfer energies of several different types of atoms using Faucheres experimental hydrophobicity scale.[23] Negative values of transfer energies correspond to hydrophobic atoms, while positive transfer energies correspond to hydrophilic atoms. The positions of the three deuterated leucine sidechains were moved to the experimental depths in the bilayer and held constant for the duration of the calculations. The peptide was rotated to all available orientations that fit the constraint of the 3 deuterated leucine depths, where the energy was then calculated. The energy, Eqn 15, associated with each possible orientation was calculated by multiplying the solvent accessible surface area (S), the transfer energy (E^{tr}), and the penalty function (C(z)) of each atom (i) and summed over all atoms (N) of the peptide.

$$E = \sum_{i=1}^{N} S_i E_i^{tr} C(z_i) \tag{15}$$

3. Results

Oriented membrane multilayers were adsorbed to silicon single crystal substrates and hydrated in a 85% relative humidity environment. When exposed to a monochromatic neutron beam, 4-5 quasi-Bragg peaks were observed which corresponded to the lamellar repeat spacings (d $\approx$ 50 – 54 Å) for the different membranes. In order to achieve the desired label resolution a minimum of 4 Bragg peaks are required,[24] therefore samples which were not aligned enough to fit this criterion were remade and resampled. A single repeat-spacing was observed for the sample (i.e. a single Bragg peak at each Bragg angle) suggesting the phospholipids did not experience phase separation. Figure 3 is a sample of a typical diffraction pattern, with a rocking curve in the inset. A rocking curve is used to evaluate the quality of sample alignment. The Figure 3 rocking curve displays a sharp peaking corresponding to large in-plane domains of highly oriented bilayers, the minima located at $\sim$0° and $\sim$-2.5° are due to the sample attenuation of the scattered and incident beams respectively.

The neutron scattering length density (NSLD) profile is the spacial visualization of the neutron scattering length distribution of a bilayer (unit cell). A unit cell contains one bilayer and the origin of the abscissa corresponds to the bilayer centre. Figure 4 (right panel) illustrate half of the centrosymmetric unit cell. The inter-layer water is located at the edges of the unit cell (Figure 4, right panels) The maxima of the black and red lines (Figure 4, right panel) at $\sim$ 16 Å roughly indicate the position of the glycerol-ester backbone of the lipid (sn-3 position). The distance between these peaks approximately defines the bilayer hydrophobic thickness,[25] and the dip in NSLD at the bilayer centre is the result of disordered (i.e., increased motion) terminal methyl groups, and where the greatest density of hydrogen occurs. The bilayer thickness (SLD profile peak–peak distance) for both DPPC:POPG and POPC:POPG lipid systems are $\sim$38 Å thick, which is in the range of POPC, POPG and DPPC,[25,26] however the presence of 5 mol% KL_4 will have a significant effect on the bilayer thickness as well as the fact that the bilayer is a phospholipid mixture. The physical properties of the bilayers studied are summarized in Table 1.

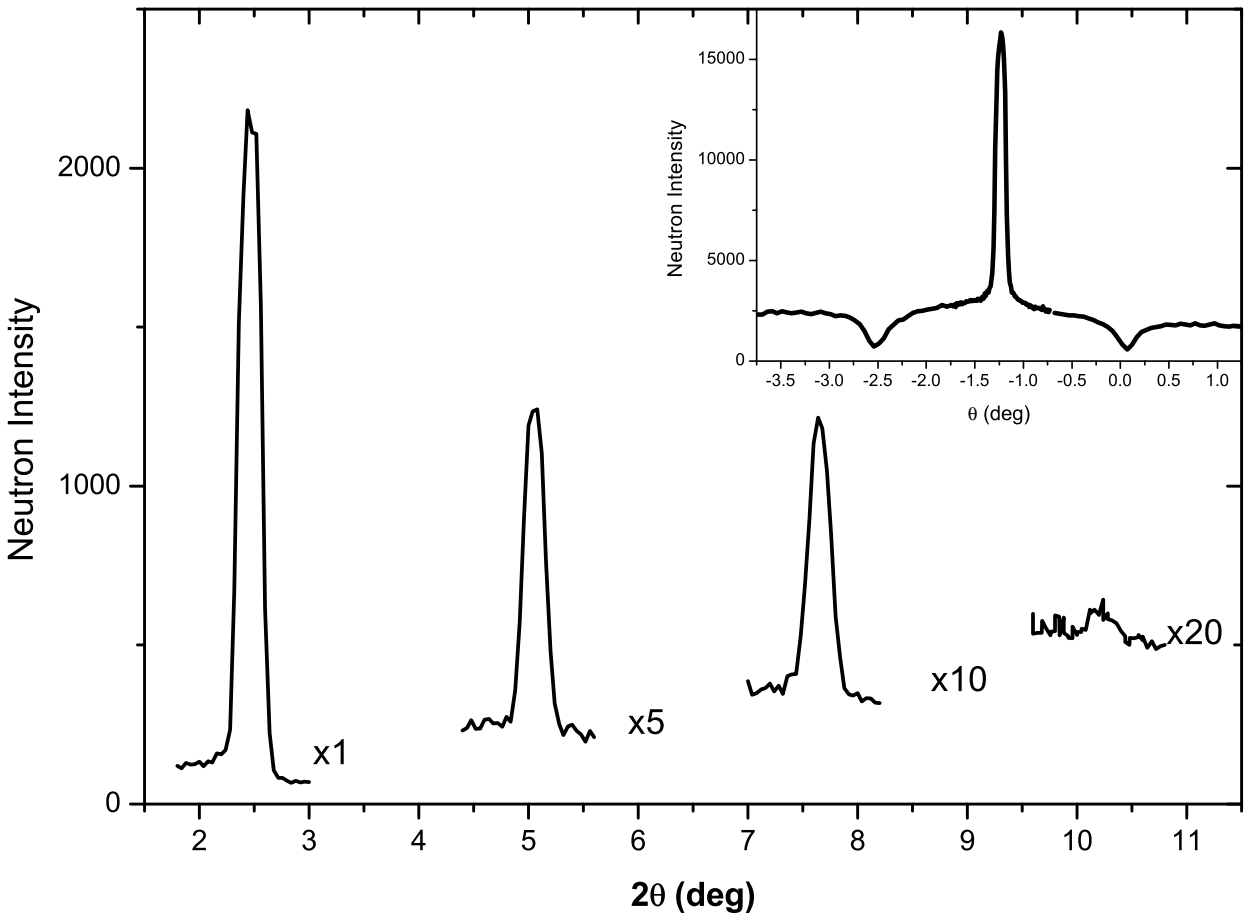

Figure 3: Main: Raw neutron diffraction data collected on the L3-labeled sample at the 8% D_2O contrast. Inset: A typical rocking curve (i.e., where the sample position, θ, is fixed and the detector angle, 2θ, is scanned) is used to indicate the alignment quality of a sample. This rocking curve is for the L3-labeled sample at the 70% D_2O.

Table 1: Physical Properties of the Bilayer

Lipid Mixture	Unit Cell	Bilayer Thickness	Water 1/e
DPPC:POPG	53.2±0.1 Å	38.2±0.2 Å	18.4±0.2 Å
DPPC:POPG*	50.1±0.1 Å	35.4±0.3 Å	15.2±0.2 Å
POPC:POPG	51.8±0.5 Å	38.4±0.2 Å	13.8±0.3 Å

Distances are referenced to the bilayer centre.

* L19 label sample and control prepared on a separate beam time allocation.

3.1 DPPC:POPG (4:1)

Among the five oriented samples (2 unlabeled and 3 labeled) the average water penetration depth was 18.4 Å from the bilayer centre. Unlabeled samples consisted of protiated KL_4 acting as a control, where as the 3 labelled samples consisted of deuterated KL_4 at L3, L12, and L19 locations (L19 data was run on a separate beam time than L3 and L12, and hence required a second unlabeled control sample). The water penetration is pivotal in the orientation optimization via hydrophobic interaction. The repeat spacing of the L3 and L12 labeled, and the unlabeled control samples was 53.2 Å (±0.1 Å). The L19 label and respective unlabeled control had a repeat spacing of 50.1 Å (±0.1 Å)[1]. Although the L19 sample was only 6% thinner than the other labels, this samples label distribution was not used as a fixed point for the orientation optimization procedure. However the distributions were used to evaluate the optimization results (*vide infra*). The experimentally determined label location for the L3, L12, and L19 labeled KL_4 in DPPC:POPG bilayers are summarized in Table 2 and illustrated in Figure 3. The two populations of the L19 label distribution are consistent with the existence of two orientations (major and minor) proposed from past NMR results,[11] with further information about the orientation of KL4 being represented in Table 3.

Table 2: KL_4 label locations in DPPC:POPG (4:1)

Label	Distribution Centre	Distribution Width	Model χ^2	R_{mod}
L3	24.1 Å	4.5 Å	0.0208	0.303
L12	18.2 Å	8.3 Å	0.179	0.291
L19*	16.2 Å	4.5 Å	0.0096	0.11

Distances are referenced to the bilayer centre.
* L19 label sample and control prepared on a separate beam time allocation.

[1]The L19 sample was collected at a later date

Table 3: KL_4 orientations in DPPC:POPG (4:1)

Helix	Insertion angle	Energy	L19 Location*
α	58 ^{o}	-13.76	7.6 Å
Major	31^o	-12.49	12.79 Å
Minor	33^o	-11.81	4.09 Å

* Distance from bilayer centre.

3.2 POPC:POPG (4:1)

Among the 3 oriented samples (1 unlabeled and 2 labeled) the average water penetration depth was 13.8 Å from the bilayer centre. This penetration is slightly deeper than the penetration of water in the DPPC:POPG samples. This is reasonable considering intrinsic disorder of POPC versus DPPC at physiological temperatures.[27,28] This is consistent with DSC data, which shows a 3:1 DPPC:POPG system with added KL_4 exists predominantly in the gel phase at physiological temperatures.[29]

The repeat spacing of the L3 and L12 labeled, and the unlabeled control samples was 51.8 Å (±0.5 Å). The L3 and L12 distributions were used to evaluate the optimization results (*vide infra*). The experimentally determined label location for the L3, and L12 labeled KL_4 in POPC:POPG bilayers are summarized in Table 4, as well as further information about KL_4 orientation, such as insertion angle and energy, are visualized in Table 5.

Table 4: KL_4 label locations in POPC:POPG (4:1)

Label	Distribution Centre	Distribution Width	Model χ^2	R $_{mod}$
L3a*	24.5 Å	3.1 Å	0.00103	0.0556
L3b*	14.3 Å	3.3 Å	0.00103	0.0556
L12	17.5 Å	9.1 Å	0.00173	0.200

* Distributions were generated from a single fit of 2 Gaussian distributions. Relative populations were 1:1 (a:b)

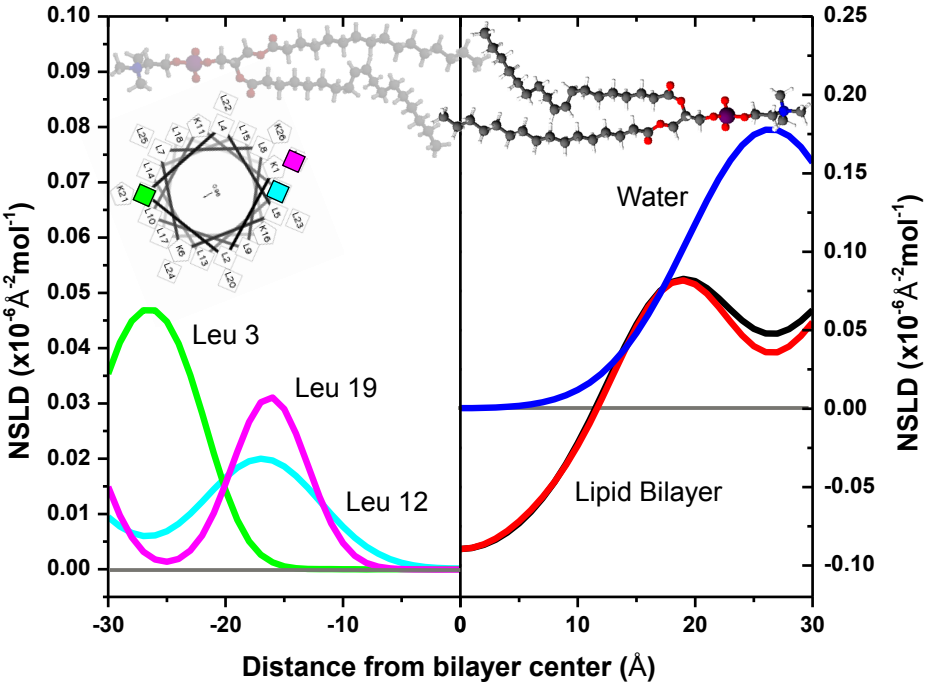

Figure 4: Left: L3, L12 and L19 label distributions as determined by oriented neutron diffraction in DPPC:POPG (4:1) bilayers. Right: NSLD profiles for DPPC:POPG with unlabeled KL_4 (red) and L12-KL_4 (black) as well as the penetration of water (blue).

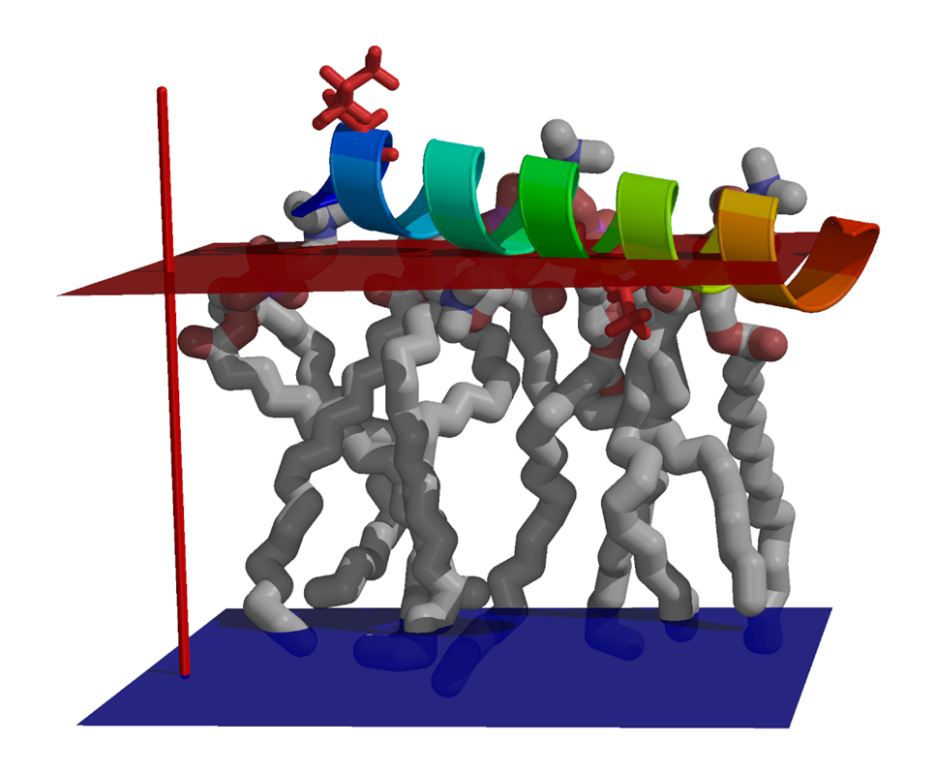

Figure 5: Pictoral rendition of KL_4's orientation with respect to the membranes surface, as determined by ^2H labels and calculated orientation optimization.

Table 5: KL_4 orientations in POPC:POPG (4:1)

	Population 1		Population 2	
Helix	Insertion angle	Energy	Insertion angle	Energy
α	62 ^{o}	+4.85	27 ^{o}	-22.38
Major	39^o	-4.18	8^o	-41.35
Minor[a]	-	+15.75	-	-27.32

[a] Minor conformer is a random coil, therefore has no helix to orient to the bilayer, while the major conformer is an alpha helix.[11]

4. Discussion

Pulmonary surfactant is a mixture of both lipids and proteins that make up an active monolayer at the air—liquid interface of alveoli, with many associated bilayers systems in its close proximity, that serves as a reservoir for excess of these biomolecules.[30] One of the more important proteins that is trying to be mirrored by KL_4 is SP-B. However, there are substantial differences in the size of native SP-B in relation to KL_4. Native SP-B is made up of 79 amino acids compared to the 21 amino acids that make up KL_4, however in many cases SP-B can be divided into a few specific functional fragments.[31,32] There have been lots of studies that focus around the first 25 amino acids of SP-B, also known as SP-B_{1-25}, which plays a significant role in the function of SP-B.[33] However, interestingly it is the final 21 amino acids of the C-terminus, SP-B_{59-79}, that were of interest when designing KL_4, specifically the ratio of charged and hydrophobic residues, and the hydrophilic/hydrophobic pattern, when compared to the C-terminus of SP-B.[13,33]

However, although the KL_4 has a rather similar hydrophobic residue to cationic residue ratio when compared to SP-B, it is important to compare how both peptides orient themselves in a PS monolayer and ultimately how they behave in such a dynamic system. Recent findings using X-ray diffuse scattering and molecular dynamic simulations have shown that SP-B tends to reside on level with the headgroups of the monolayer with some of the peptide intruding into the hydrocarbon core.[34] This data, along with the previous results, helps elucidate the possibility that KL_4 acts as a SP-B mimic, not only because the similar framework characteristics of the two peptides, but also due to the similar orientation within monolayer

systems resembling PS, although not exactly identical.

This also goes to further contest the opposing view of various groups of KL_4 being a transmembrane protein, specifically that KL_4 has a more similar orientation to the native transmembrane protein, SP-C.[34,35] In vitro studies show that SP-C plays a role in PS recycling, as well surface tension lowering qualities.[35] Therefore, SP-C also is an important protein within the system of PS, and is also added to various therapeutic surfactant therapies. However the results presented in this paper regarding the orientation of KL_4, go against this idea, and promote the initial thought of this paper, that KL_4 is a SP-B replacement.

Our results demonstrate that the peptide KL_4 interacts with only one leaflet of the bilayer at a time (monotopic), this result is consistent with a orientation which is amenable to a phospholipid monolayer. Thus the notion believed by some groups that KL_4 adopts a transmembrane orientation (polytopic) seems counter-intuitive when considering the basic structure of a monolayer. Our monotopic picture of KL_4, illustrated in Figure 5, is also consistent with work completed by Turner et al., using electron spin resonance (ESR) power saturation, that KL_4 resides with the helical axis perpendicular to the bilayer normal.[36] The measured backbone angles from our NMR-generated model have augmented the belief that the peptide exists with helical character in different lipid environments, such as systems composed mainly of DPPC or POPC. For example work done by Mills et al. show evidence of its helical nature in a 4:1 POPC:POPG large unilamellar vesicles (LUVs).[37] This further establishes the theory of KL_4 keeping its structure in such lipid environments, which is of the utmost importance if it were to be used in possible medicinal pulmonary surfactant mimics.

Both lipid systems yielded KL_4 orientations which interacted with only half the bilayer, however, there were differences in pitch, number of label locations and mobility. Interestingly the peptide depth is deeper in DPPC:POPG samples, yet water penetration is deeper in POPC:POPG samples. This could be due to the potential bilayer thickness miss-match that could occur in the DPPC:POPG due to the temperature being below DPPC's main phase transition,[25,26] DSC studies suggest phase separation in DPPC:POPG samples where KL_4

concentrations were greater than 3 mol%.[11,29] Typically lipid separation driven by thickness mismatch would yield Bragg peaks corresponding to two different lamellar repeat spacings,[20] we observed Bragg peaks which correspond to a single spacing.

^{2}H-NMR studies have demonstrated the L3 label has the most mobility,[38] interestingly our neutron scattering results show a broader distribution for the L12 label than for the L3 label. A possible explanation for this discrepancy arises because ^{2}H-NMR is sensitive to motion in all three dimensions while oriented neutron diffraction specifically looks at distributions in one dimension (perpendicular to the plane of the bilayer).

^{2}H-NMR order parameters demonstrated that KL_4 introduced order along the acyl chains of DPPC [11] which is in direct alignment with our present diffraction data. These changes in order parameters indicate that KL_4 lodges into the hydrophobic region of the bilayer while maintaining its helix axis perpendicular to the bilayer normal.[11] Our optimized model is in direct alignment with conclusions drawn by Antharam *et al.*.

Structural characterization of KL_4 in different lipid environments via circular dichroism (CD) and Fourier-transform infrared spectroscopy (FTIR) consistently indicated the formation of a helical peptide conformation although some variations in helicity with lipid composition have been reported.[29,37] CD spectrum by Antharam et al. were unable to be fit by means of canonical α-helices, which agrees with the model of a unconventional helix.[11] In fact the optimized orientation yields comparable energies for the three KL_4 helices tested in DPPC:POPG, however the location of the L19 label does not agree with the location predicted by a conventional α-helix.

The conflicting literature with regards to KL_4 being a transmembrane peptide, Gustafsson et al. claim it is a transmembrane (TM) peptide in a 7:3 DPPC/PG system based on oriented FTIR and oriented CD spectroscopy.[15]Although this system is similar to the ones in this paper, the differing composition may be the reason for the difference in reported conformation. However there are other groups that also report it as transmembrane, for example Martínez-Gil et al. states a transmembrane orientation, however for a endoplasmic

reticulum (ER) membrane system. Therefore it should be noted that KL_4 has the possibility of taking on a transmembrane orientation, however for the PS systems of interest investigated in this paper it does not. Several other studies determine that KL_4 is in fact not a TM peptide.[39] Both the label locations in the neutron diffraction data and the possible length of a KL_4 helix does not lend itself to a transmembrane orientation. In fact the data suggests KL_4 sits within one leaflet of the bilayer with a tilt angle which appears to prevent interdigitation.

Thermodynamically, there are two main thoughts which are believed to drive KL_4's location in the membrane: i) the charged lysine residues interact with the phosphate/water interface minimizing the energy penalty of burying a charge in the hydrophobic core or ii) due to the large amount of leucine residues (hydrophobic) present deep penetration into the hydrophobic core would be most energetically favourable.[11] Even at a crude approximation, one can see that the energy cost of burying Leu does not surpass the gain from sequestering the Lys.[40]

These findings can further give validity to the use of KL_4 as a synthetic option to SP-B. The potential option of using it as a SP-B substitute can be of utmost importance in the area of pharmaceutical pulmonary surfactant products, as previously mentioned. SP-B is the most important protein in the monolayer surfactant system playing a vital role in the biophysical characteristics of PS, specifically in reduction of surface tension and interface adsoprtion.[5,6] It has also been shown to increase lateral stability of phospholipid layers, which likely factors into these beneficial characteristics. As well, SP-B's physiological importance is further evidenced by the fact that SP-B is the only protein that when "knocked-out" of mouse systems leads to dysfunctional PS, ultimately leading to neonatal death due to respiratory failure.[41]

Preliminary in vivo studies have been completed of a KL_4-surfactant which further builds on the narrative of its importance. A surfactant system, with a similar lipid environment to that of the experiments in this study, of 3:1 DPPC/POPG with 15wt% palmitic acid and 3 wt% KL_4, was tested on infant rhesus monkeys exhibiting respiratory distress to

highlight its efficacy as a potential therapeutic SP-B analog.[32] A formula very similar to the composition of Lucinactant, a pharmaceutical surfactant therapeutic. Groups which received the KL_4 containing surfactant showed much higher alveolar oxygen partial pressure than those receiving a surfactant devoid of any of the peptide.[32] A bubble surfactometer study was also used to investigate surface tension. KL_4-surfactant showed the ability to lower surface tension to similar values of endogenous PS, while also outperforming phospholipid-only surfactants.[32] It is important to note that this composition contains palmitic acid which may alter the orientation of KL_4 compared to the environments tests within this study, but nevertheless still emphasizes the importance of KL_4 as a therapeutic. Therefore there is evidence to support KL_4 having utility in surfactant systems to benefit physiological processes, however it still needs to be determined if this utility is because of homologous characteristics to SP-B.

Another area where KL_4 can also prove to exist with a possible important function in the area of drug delivery, specifically as a carrier for small interfering RNA (siRNA). siRNA, a type of nucleic acid, are shown to have promising beneficial effects combating against many medical conditions, ranging from lung cancer to influenza.[42] Since nucleic acids are known for their characteristic negative charge, the thought of using a cationic KL_4 protein as a carrier for siRNA resonates as a realistic option. Qiu et al. shows that using KL_4 to complex with siRNA as a carrier to be a viable option, with it having comparable, if not better, transfection rates compared to Lipofectamine 2000, while also not presenting any overall cytotoxic capabilities ($> 95\%$ cell viability).[42] However further research with KL_4 would need to be done in this area of study.

5. CONCLUSIONS

We propose a location and orientation of peptide KL_4 in both DPPC:POPG and POPC:POPG bilayers by neutron scattering and computational optimization. In both phospholipid com-

positions we observe the helical axis of KL_4 lies approximately perpendicular to the bilayer normal. We note this orientation can also be adopted in a monolayer system, as in the case of pulmonary surfactant.

Acknowledgement

The authors wish to acknowledge the Canadian Neutron Beam Centre (CNBC, Chalk River, ON) for providing a generous amounts of neutron beamtime. D.M. and T.A.H. is partially supported by National Science and Engineering Research Council of Canada (NSERC). J.R.L. was partially supported by the Gates Foundation. The assistance of Dr. Alfred Chung in peptide synthesis is gratefully acknowledged.

References

(1) Goerke, J. Pulmonary surfactant: functions and molecular composition. *Biochimica et Biophysica Acta (BBA) - Molecular Basis of Disease* **1998**, *1408*, 79 – 89.

(2) Rodriguez, R. J. Management of Respiratory Distress Syndrome: An Update. *Respiratory Care* **2003**, *48*, 279–287.

(3) Agudelo, C. W.; Samaha, G.; Garcia-Arcos, I. Alveolar lipids in pulmonary disease. A review. *Lipids in health and disease* **2020**, *19*, 1–21.

(4) de la Serna, J. B.; Hansen, S.; Berzina, Z.; Simonsen, A. C.; Hannibal-Bach, H. K.; Knudsen, J.; Ejsing, C. S.; Bagatolli, L. A. Compositional and structural characterization of monolayers and bilayers composed of native pulmonary surfactant from wild type mice. *Biochimica et Biophysica Acta (BBA) - Biomembranes* **2013**, *1828*, 2450 – 2459.

(5) Dziura, M.; Mansour, B.; DiPasquale, M.; Chandrasekera, P. C.; Gauld, J. W.; Marquardt, D. Simulated Breathing: Application of Molecular Dynamics Simulations to Pulmonary Lung Surfactant. *Symmetry* **2021**, *13*.

(6) Hawgood, S. Pulmonary surfactant apoproteins: a review of protein and genomic structure. *American Journal of Physiology-Lung Cellular and Molecular Physiology* **1989**, *257*, L13–L22.

(7) Holten-Andersen, N.; Henderson, J. M.; Walther, F. J.; Waring, A. J.; Ruchala, P.; Notter, R. H.; Lee, K. Y. C. KL4 peptide induces reversible collapse structures on multiple length scales in model lung surfactant. *Biophysical journal* **2011**, *101*, 2957–2965.

(8) MartínezCalle, M.; Olmeda, B.; Dietl, P.; Frick, M.; PérezGil, J. Pulmonary surfactant protein SPB promotes exocytosis of lamellar bodies in alveolar type II cells. *The FASEB Journal* **2018**, *32*, 4600–4611.

(9) Farver, S.; Smith, A. N.; Mills, F. D.; Egri, A. G.; Long, J. R. Delineation of the dynamic properties of individual lipid species in native and synthetic pulmonary surfactants. *Biochimica et Biophysica Acta (BBA) - Biomembranes* **2015**, *1848*, 203 – 210.

(10) Wang, S.; Li, Z.; Wang, X.; Zhang, S.; Gao, P.; Shi, Z. The role of pulmonary surfactants in the treatment of acute respiratory distress syndrome in COVID-19. *Frontiers in Pharmacology* **2021**, *12*, 1640.

(11) Antharam, V. C.; Elliott, D. W.; Mills, F. D.; Farver, R. S.; Sternin, E.; Long, J. R. Penetration Depth of Surfactant Peptide KL4 into Membranes Is Determined by Fatty Acid Saturation. *Biophysical Journal* **2009**, *96*, 4085 – 4098.

(12) Antharam, V. C.; Farver, R. S.; Kuznetsova, A.; Sippel, K. H.; Mills, F. D.; Elliott, D. W.; Sternin, E.; Long, J. R. Interactions of the C-terminus of lung surfactant

protein B with lipid bilayers are modulated by acyl chain saturation. *Biochimica et Biophysica Acta (BBA)-Biomembranes* **2008**, *1778*, 2544–2554.

(13) Martínez-Gil, L.; Pérez-Gil, J.; Mingarro, I. The surfactant peptide KL4 sequence is inserted with a transmembrane orientation into the endoplasmic reticulum membrane. *Biophysical journal* **2008**, *95*, L36–L38.

(14) Wüstneck, N.; Wústneck, R.; Perez-Gil, J.; Pison, U. Effects of Oligomerization and Secondary Structure on the Surface Behavior of Pulmonary Surfactant Proteins SP-B and SP-C. *Biophysical Journal* **2003**, *84*, 1940 – 1949.

(15) Gustafsson, M.; Vandenbussche, G.; Curstedt, T.; Ruysschaert, J.-M.; Johansson, J. The 21-residue surfactant peptide (LysLeu4)4Lys(KL4) is a transmembrane ??-helix with a mixed nonpolar/polar surface. *FEBS Letters* **1996**, *384*, 185 – 188.

(16) Marquardt, D.; Williams, J. A.; Kuerka, N.; Atkinson, J.; Wassall, S. R.; Katsaras, J.; Harroun, T. A. Tocopherol Activity Correlates with Its Location in a Membrane: A New Perspective on the Antioxidant Vitamin E. *Journal of the American Chemical Society* **2013**, *135*, 7523–7533.

(17) Marquardt, D.; Williams, J. A.; Kinnun, J. J.; Kuerka, N.; Atkinson, J.; Wassall, S. R.; Katsaras, J.; Harroun, T. A. Dimyristoyl Phosphatidylcholine: A Remarkable Exception to -Tocopherols Membrane Presence. *Journal of the American Chemical Society* **2014**, *136*, 203–210.

(18) Marquardt, D.; Harroun, T. *Liposomes, Lipid Bilayers and Model Membranes*; CRC Press, 2014; pp 199–216–.

(19) Harroun, T. A.; Katsaras, J.; Wassall, S. R. Cholesterol Hydrozyl Group Is Found To Reside in the Center of a Polyunsaturated Lipid Membrane. *Biochemistry* **2006**, *45*, 1227–1233.

(20) Kucerka, N.; Marquardt, D.; Harroun, T. A.; Nieh, M.-P.; Wassall, S. R.; de Jong, D. H.; Schafer, L. V.; Marrink, S. J.; Katsaras, J. Cholesterol in Bilayers with PUFA Chains: Doping with DMPC or POPC Results in Sterol Reorientation and Membrane-Domain Formation. *Biochemistry* **2010**, *49*, 7485–7493.

(21) Harroun, T. A.; Katsaras, J.; Wassall, S. R. Cholesterol Is Found To Reside in the Center of a Polyunsaturated Lipid Membrane. *Biochemistry* **2008**, *47*, 7090–7096, PMID: 18543943.

(22) Hamilton, W. C. Significance tests on the crystallographic *R* factor. *Acta Crystallographica* **1965**, *18*, 502–510.

(23) Ducarme, P.; Thomas, A.; Brasseur, R. The optimisation of the helix/helix interaction of a transmembrane dimer is improved by the {IMPALA} restraint field. *Biochimica et Biophysica Acta (BBA) - Biomembranes* **2000**, *1509*, 148 – 154.

(24) Gordeliy, V. I.; Chernov, N. I. Accuracy of Determination of Position and Width of Molecular Groups in Biological and Lipid Membranes via Neutron Diffraction. *Acta Crystallographica D* **1997**, *D53*, 377–384.

(25) Norbert Kucerka, J. K., Mu-Ping Nieh Fluid phase lipid areas and bilayer thicknesses of commonly used phosphatidylcholines as a function of temperature. *Biochimica et Biophysica Acta* **2011**, *1808*, 2761–2771.

(26) Pan, J.; Heberle, F. A.; Tristram-Nagle, S.; Szymanski, M.; Koepfinger, M.; Katsaras, J.; Kucerka, N. Molecular structures of fluid phase phosphatidylglycerol bilayers as determined by small angle neutron and X-ray scattering. *BIOCHIMICA ET BIOPHYSICA ACTA-BIOMEMBRANES* **2012**, *1818*, 2135–2148.

(27) Nagarajan, S.; Schuler, E. E.; Ma, K.; Kindt, J. T.; Dyer, R. B. Dynamics of the gel to fluid phase transformation in unilamellar DPPC vesicles. *The Journal of Physical Chemistry B* **2012**, *116*, 13749–13756.

(28) Rappolt, M.; Vidal, M.; Kriechbaum, M.; Steinhart, M.; Amenitsch, H.; Bernstorff, S.; Laggner, P. Structural, dynamic and mechanical properties of POPC at low cholesterol concentration studied in pressure/temperature space. *European Biophysics Journal* **2003**, *31*, 575–585.

(29) Sáenz, A.; Cañadas, O.; Bagatolli, L. A.; Johnson, M. E.; Casals, C. Physical properties and surface activity of surfactant-like membranes containing the cationic and hydrophobic peptide KL4. *FEBS Journal* **2006**, *273*, 2515–2527.

(30) Baoukina, S.; Tieleman, D. P. Lung surfactant protein SP-B promotes formation of bilayer reservoirs from monolayer and lipid transfer between the interface and subphase. *Biophysical journal* **2011**, *100*, 1678–1687.

(31) Curstedt, T.; Johansson, J.; Persson, P.; Eklund, A.; Robertson, B.; Löwenadler, B.; Jörnvall, H. Hydrophobic surfactant-associated polypeptides: SP-C is a lipopeptide with two palmitoylated cysteine residues, whereas SP-B lacks covalently linked fatty acyl groups. *Proceedings of the National Academy of Sciences* **1990**, *87*, 2985–2989.

(32) Revak, S. D.; Merritt, T. A.; Cochrane, C. G.; Heldt, G. P.; Alberts, M. S.; Anderson, D. W.; Kheiter, A. Efficacy of synthetic peptide-containing surfactant in the treatment of respiratory distress syndrome in preterm infant rhesus monkeys. *Pediatric research* **1996**, *39*, 715–724.

(33) Braide-Moncoeur, O.; Tran, N. T.; Long, J. R. Peptide-based synthetic pulmonary surfactant for the treatment of respiratory distress disorders. *Current opinion in chemical biology* **2016**, *32*, 22–28.

(34) Loney, R. W.; Panzuela, S.; Chen, J.; Yang, Z.; Fritz, J. R.; Dell, Z.; Corradi, V.; Kumar, K.; Tieleman, D. P.; Hall, S. B. Location of the hydrophobic surfactant proteins, SP-B and SP-C, in fluid-phase bilayers. *The Journal of Physical Chemistry B* **2020**, *124*, 6763–6774.

(35) Mulugeta, S.; Beers, M. F. Surfactant protein C: its unique properties and emerging immunomodulatory role in the lung. *Microbes and infection* **2006**, *8*, 2317–2323.

(36) Turner, A. L.; Braide, O.; Mills, F. D.; Fanucci, G. E.; Long, J. R. Residue specific partitioning of KL4 into phospholipid bilayers. *Biochimica et Biophysica Acta (BBA) - Biomembranes* **2014**, *1838*, 3212 – 3219.

(37) Mills, F. D.; Antharam, V. C.; Ganesh, O. K.; Elliott, D. W.; McNeill, S. A.; Long, J. R. The Helical Structure of Surfactant Peptide KL4 When Bound to POPC: POPG Lipid Vesicles. *Biochemistry* **2008**, *47*, 8292–8300.

(38) Long, J. R.; Mills, F. D.; Ganesh, O. K.; Antharam, V. C.; Farver, R. S. Partitioning, dynamics, and orientation of lung surfactant peptide {KL4} in phospholipid bilayers. *Biochimica et Biophysica Acta (BBA) - Biomembranes* **2010**, *1798*, 216 – 222, ¡ce:title¿Membrane Protein Dynamics by NMR: Correlation of Structure and Function¡/ce:title¿.

(39) Cai, P.; Flach, C. R.; Mendelsohn, R. An Infrared Reflection???Absorption Spectroscopy Study of the Secondary Structure in (KL4)4K, a Therapeutic Agent for Respiratory Distress Syndrome, in Aqueous Monolayers with Phospholipids??? *Biochemistry* **2003**, *42*, 9446–9452, PMID: 12899632.

(40) Chan, H. S. *Encylcopedia of Life Sciences*; Macmillan Publishers Ltd, 2002.

(41) Weaver, T. E.; Beck, D. C. Use of knockout mice to study surfactant protein structure and function. *Neonatology* **1999**, *76*, 15.

(42) Qiu, Y.; Chow, M. Y. T.; Liang, W.; Chung, W. W. Y.; Mak, J. C. W.; Lam, J. K. W. From pulmonary surfactant, synthetic KL4 peptide as effective siRNA delivery vector for pulmonary delivery. *Molecular pharmaceutics* **2017**, *14*, 4606–4617.

Graphical TOC Entry